Since January 2020 Elsevier has created a COVID-19 resource centre with free information in English and Mandarin on the novel coronavirus COVID-19. The COVID-19 resource centre is hosted on Elsevier Connect, the company's public news and information website.

Bioelectrochemistry 147 (2022) 108161

Contents lists available at ScienceDirect

Bioelectrochemistry

journal homepage: www.journals.elsevier.com/bioelectrochemistry

Development of sandwich electrochemiluminescence immunosensor for COVID-19 diagnosis by SARS-CoV-2 spike protein detection based on Au@BSA-luminol nanocomposites

Morteza Hosseini [a,*], Ebtesam Sobhanie [a], Foad Salehnia [a], Guobao Xu [b], Hodjattallah Rabbani [c], Mahsa Naghavi Sheikholeslami [d], Ali Firoozbakhtian [a], Niloufar Sadeghi [c], Mohammad Hossein Farajollah [e], Mohammad Reza Ganjali [d], Houman Vosough [e]

[a] Nanobiosensors Lab, Department of Life Science Engineering, Faculty of New Sciences & Technologies, University of Tehran, Tehran, Iran
[b] State Key Laboratory of Electroanalytical Chemistry, Changchun Institute of Applied Chemistry, Chinese Academy of Sciences, Changchun 130022, China
[c] Monoclonal Antibody Research Center, Avicenna Research Institute, ACECR, Tehran, Iran
[d] Center of Excellence in Electrochemistry, School of Chemistry, University of Tehran, Tehran, Iran
[e] Clinical Labs, Farhikhtegan Hospital, Tehran, Iran

ARTICLE INFO

Keywords:
SARS-CoV-2
COVID-19
Electrochemiluminescence
Sandwich immunosensor
Au@BSA-luminol

ABSTRACT

Coronavirus disease (COVID-19) is a new and highly contagious disease posing a threat to global public health and wreaking havoc around the world. It's caused by the Coronavirus that causes severe acute respiratory syndrome (SARS-CoV-2). In the current pandemic situation, rapid and accurate SARS-CoV-2 diagnosis on a large scale is critical for early-stage diagnosis. Early detection and monitoring of viral infections can aid in controlling and preventing infection in large groups of people. Accordingly, we developed a sensitive and high-throughput sandwich electrochemiluminescence immunosensor based on antigen detection for COVID-19 diagnosis (the spike protein of SARS-CoV-2). For the spike protein of SARS-CoV-2, the ECL biosensor had a linear range of 10 ng mL^{-1} to 10 μg mL^{-1} with a limit of detection of 1.93 ng mL^{-1}. The sandwich ECL immunosensor could be used in early clinical diagnosis due to its excellent recovery in detecting SARS-CoV-2, rapid analysis (90 min), and ease of use.

1. Introduction

The new acute respiratory syndrome coronavirus 2 (SARS-CoV-2) outbreak put people's physical and mental health all over the world in danger. The virus's rapid transmission speed and high infectious capacity have resulted in a considerable increase in the number of affected people every day. As a result, early detection of SARS-CoV-2 is critical for human survival, health, and security. Early clinical diagnosis of SARS-CoV-2 is quite challenging. The gold standard method of RT-PCR requires complex types of equipment as well as skilled personnel, resulting in a costly and sensitive assay. The procedure requires sample pretreatment as it operates on the genome of the virus [1,2]. Elimination of the many steps involved not only lessens the duration of the process but also reduces the chance of human error in it. This would also eliminate the need for trained personnel and cut expenses. Biosensors as highly sensitive, selective, and accurate monitoring tools are the alternatives to the traditional methods of detection. These sensors are capable of ultralow determination of analytes in biological samples. Among them, electrochemical biosensors have the advantages of ultrasensitive detection and a wide range of detection [3,4].

Electrochemiluminescence (ECL)-based sensors are classified as one of electrochemical sensors featuring good sensitivity as well as stability. ECL technology has become more popular in recent years as a strong analytical technique for the detection of biomolecules in clinical, environmental, and industrial settings [5–7]. The ECL method has also been used in the analysis of disease-related biomarkers. It offers high sensitivity, low cost, simple operation, and easy miniaturization and intelligence to answer clinical treatment development needs [8,9].

The antigen–antibody specific interactions are considered as one of the most selective and sensitive interactions. The employment of antibodies as bioreceptors in immunosensors is responsible for the high sensitivity and selectivity of these types of sensors enabling ultra-low

* Corresponding author.
E-mail address: smhosseini@khayam.ut.ac.ir (M. Hosseini).

https://doi.org/10.1016/j.bioelechem.2022.108161
Received 12 February 2022; Received in revised form 11 April 2022; Accepted 14 May 2022
Available online 25 May 2022

detection of analytes in biological samples. Immunosensors detect antibody binding to a specific target molecule and can be used to detect the presence and quantity of specific antibodies in order to find whether a patient has been previously infected and to assess the disease's prevalence [10–12]. The most common detection strategy in immunosensors is the sandwich immunoassay type. The detected antigen is sandwiched between two antibodies, one of which, the capture antibody, is attached to the transducer surface. On the other hand, the detection antibody is usually labeled through which the amount of antigen is measured [13,14].

Smartphone-based sensing systems have recently received much attention since they provide a semi-automated user interface that even non-technical individuals can utilize [15]. Sensing systems can be designed within a smartphone with customized hardware and software incorporated, allowing the system to be miniaturized and carried out in any location. They can be operated by anyone who is semi-trained [16,17]. The RGB[1] color space is regarded as the most expanded and accepted color system. Virtually every visible spectrum can be represented as RGB three colors in a mixture of different proportions and intensities [18–20].

Noble metal nanocomposites have been used in ECL-based detections of biomarkers due to their low toxicity and enhancing effects on the ECL signal. In research done by Jia's team, Ag@BSA-luminol-Ab_2 nanocomposites were employed for the detection of carbohydrate antigen 19-9 [21]. Another ECL-based biosensor for the detection of human chorionic gonadotropin was reported [22]. The sensor benefits from a sandwich assay signaling format employing Au star@BSA-luminol-Ab_2 as the signal reporter. The great water solubility and low toxicity of the nanocomposites combined with their enhancing effect on the ECL intensity of the luminol have made them a good candidate for this work.

Here, for the first time we report the ECL-based detection of SARS-CoV-2 in a signal-on sensing format in untreated samples through its surface spike proteins. The immunosensor was fabricated by the addition of gold nanoparticles (AuNPs), 11-mercapto undecanoic acid (MUA), and 3-mercapto propionic acid to a glassy carbon electrode surface. The Ab_1 was then immobilized on the surface of the electrode through 1-(3-dimethylaminopropyl)-3-ethylcarbodiimide hydrochloride (EDC) and N-hydroxysuccinimide (NHS) functionalization of the electroe. The detecting antibodies (Ab_2) and luminous substance luminol were immobilized using flower-like Au@BSA nanoparticles with excellent biocompatibility. The determination steps were evaluated using the development of an immunocomplex between the antigen and the ECL labeled antibody. Moreover, visual detection of targets based on Smartphone Imaging is being investigated for future application of this system.

2. Materials and methods

2.1. Chemicals and apparatus

N-hydroxysuccinimide (NHS), 1-(3-dimethylaminopropyl)-3-ethylcarbodiimide hydrochloride (EDC) and bovine serum albumin (BSA), 3-mercapto propionic acid (MPA) 99%, 11-mercapto undecanoic acid (MUA) 95%, gold (III) chloride hydrate ($HAuCl_4{\cdot}4H_2O$, 99%), potassium ferrocyanide ($K_4Fe(CN)_6$), potassium chloride (KCl), luminol ($C_8H_7N_3O_2$) and hydrogen peroxide (H_2O_2) were purchased, from Sigma Aldrich. Sodium borohydride ($NaBH_4$), sodium citrate, and glutaraldehyde (25%) were obtained from Merck Chemical Co.

The polyclonal antibody anti-SARS-CoV (made in rabbit, 1.3 mg mL^{-1}) (Ab_1), as well as the polyclonal antibody SARS-CoV Spike (manufactured in goat, 1.8 mg mL^{-1}) (Ab_2), which identifies the S protein, were bought from Padzacompany (Iran). Inactivated virus (vero cell) vaccine (Coronavac; Sinovac, 1 mg mL^{-1}). Antigens and antibodies were prepared and diluted in PBS 1X buffer, pH 7.4.

2.2. Apparatus

A three-electrode setup was used for all electrochemical and ECL studies, with the modified glassy carbon electrode (GCE, 2 mm) serving as the working electrode, a saturated KCl Ag/AgCl electrode serving as the reference electrode, and a Pt wire serving as an auxiliary electrode. A DropSens Stat400 Bipotentiostat/Galvanostat was used to perform cyclic voltammetry (CV) analyses (Asturias, Spain). A photomultiplier LS 50 (Perkin-Elmer) was coupled to operate as an ECL detector with a bias potential of −800 V. The working electrode was vertically placed in a 4 mL quartz cell for the ECL measurements. The AUTOLAB PGSTAT 30 was used to perform electrochemical impedance spectroscopy (EIS) experiments (The Netherlands). A Metrohm device was used to take the pH readings. Microscopy images and morphology studies were obtained using a MIRA3 TESCAN-XMU Scanning Electron Microscope.

2.3. Preparation of Flower-like Au@BSA nanomaterials

The Au nanoparticles employed in the synthesis process were obtained according to previously published work with minimal modifications [23,24]. Briefly, 5 mL trisodium citrate solution (38 mM) was added to 25 mL boiling $HAuCl_4$ (1 mM) solution under constant stirring for 8–10 min until the color of the solution changed to red wine, indicating the practical synthesis of gold seeds. Following that, BSA was used to create various functional groups via the interaction of thiol groups with Au nanomaterials. Freshly generated BSA solution (500 mg) was first denatured by reacting with the chemical reagent sodium borohydride (40 mg) with vigorous stirring for one night to transform the disulfide bonds into thiol groups and generate additional thiol groups onto the surface of BSA [21,22]. After that, the obtained products were centrifuged and washed multiple times with double-distilled water and ethanol, respectively. Before usage, the compounds were freeze-dried and stored at 4 °C in the refrigerator.

2.4. Synthesis of luminol and Ab_2 labeled Au@BSA (luminol-Au@BSA-Ab_2):

The luminol and Ab_2 modified Au@BSA were produced using the chemical bonding approach in this study. Ultrasonication was used to dissolve 2 mg of Au@BSA into 1 mL double-distilled water. After that, 400 μL of 12.5% GA was promptly added to the above solution and shaken for 3 h to ensure GA was attached to the Au@BSA surface. Subsequently, the GA-linked Au@BSA was centrifuged and rinsed several times with double-distilled water to remove unreacted chemicals before dissolved in 1 mL PBS (0.1 M, pH 7.4). A 0.05 M luminol solution was added to the above solution and shaken for 4 h. The resulting Au@BSA-luminol nanocomposites were centrifuged and washed in 2 mL 0.1 M PBS (pH 7.4) containing 2 mg EDC and 2 mg NHS and shaken for 2 h to activate the carboxylic groups on the surface of BSA. Finally, 40 μ L detection antibodies (1.8 mg mL^{-1}) were added to the mixture and stirred slowly for 8 h in an ice bath to effectively conjugate the Ab_2 to the surface of the Luminol-Au@BSA. The produced luminol-Au@BSA-Ab_2 nanocomposites were separated by centrifugation (6000 rpm) and washed with double-distilled water to eliminate any remaining reagents. The produced luminol-Au@BSA-Ab_2 nanomaterials were dispersed in 1 mL PBS (0.1 M, pH 7.4) for further application.

2.5. ECL immunosensor preparation

A 0.05 M alumina slurry was used to polish the GCE (2 mm). After that, the mirror-like surface was cleaned with distilled water and allowed to dry at room temperature. By immersing the electrode in an electrochemical cell containing a solution of 10 mg mL^{-1} $HAuCl_4$ in 0.1 M KNO_3, followed by a 60-second potential step of −0.2 V, AuNPs were

[1] [1] Red-Green-Blue

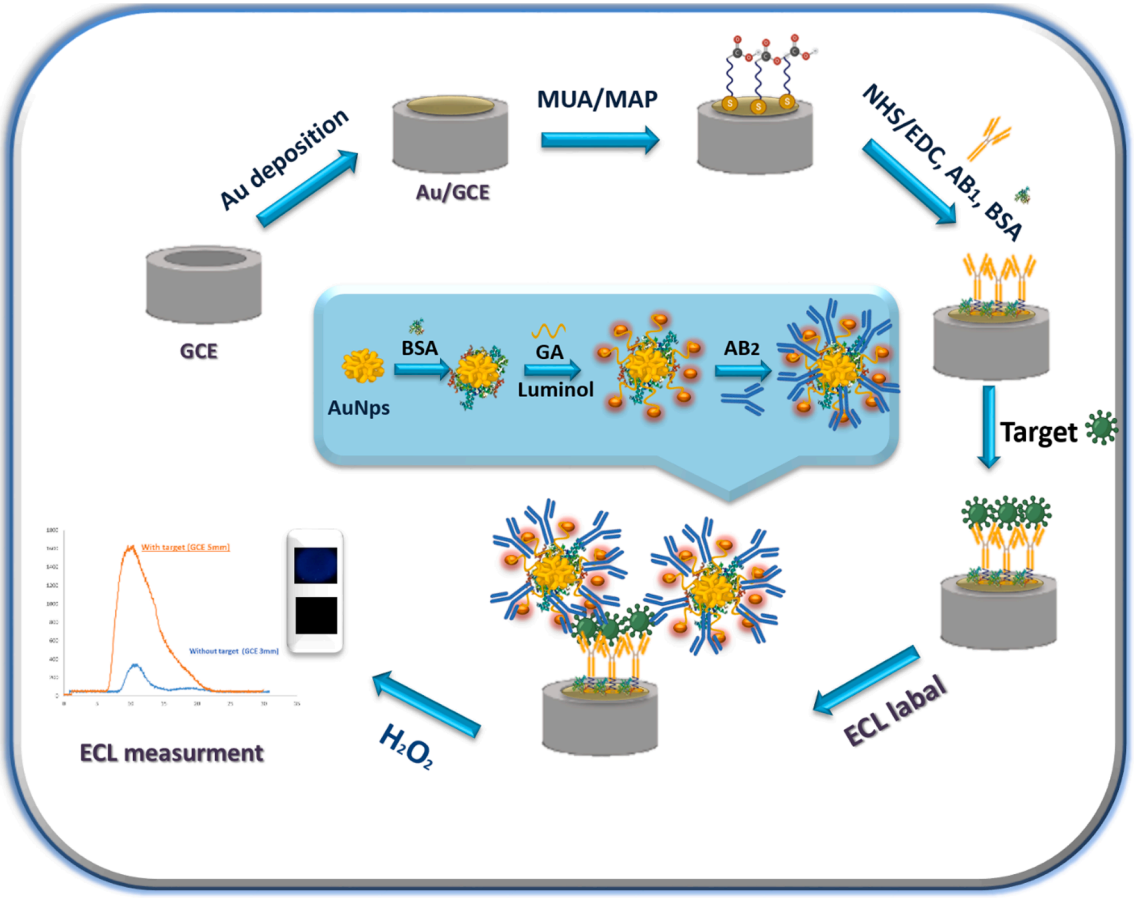

Scheme 1. Schematic illustration of the sandwich ECL immunosensor based on Au@BSA-luminol ECL biosensor for the assay SARS-CoV-2 antigen.

deposited on the electrode surface. Then, the electrode was washed with distilled water and dried at room temperature. The AuNPs/GC electrode was then immersed in a solution comprising MPA (20 mM) and MUA (20 mM) in a 10:1 mol ratio for an overnight period. The following day, the electrode was washed in PBS solution to remove unattached molecules before being immersed in EDC-NHS solution for 1 h to activate the carboxyl groups in preparation for additional attachment to the protein amine groups. It was then dried after being rinsed with PBS (pH = 7.4) solution. Following that, for immobilization of the antibody, 4μ l of the Ab_1 solution (13μ g mL^{-1}) in PBS 1X was dropped on the electrode surface and incubated for 1 h, after which the electrode was washed with PBS to eliminate any possible extra molecules. Finally, the constructed immunosensor was incubated for 45 min with 4μ l of BSA (1%) in PBS (pH = 7.4) to prevent non-specific binds and blockage of unreacted sites. Before the detection step, the electrode was properly cleansed with PBS (pH 8.5) before the detection procedure. Scheme 1 depicts the ECL immunosensor fabrication process.

2.6. ECL measurement of SARS-CoV-2 antigen

4 μL of SARS-CoV-2 antigen solution with different concentrations were dropped on the constructed immunosensor for 1 h, followed by a thorough washing with the same buffer to eliminate any unbound antigens. The modified electrodes were further modified with 4 μL luminol-Au@BSA-Ab_2 solution at 37 °C for 1 h. Finally, the immunosensor was rinsed in PBS and kept at 4 °C for further use. The ECL signals were recorded by cyclic voltammetry (CV) with a 0–1 V scanning range at 100 mV s^{-1}

3. Results and discussion

3.1. Characterization of flower-like Au@BSA nanoparticles

FESEM was used to investigate the morphology and nanostructure of flower-like Au@BSA nanoparticles. The nanoparticles had a flower-like structure with an average size of about 80 nm and were coated with a BSA layer, as shown in Fig. 1A. The flower-like Au@BSA nanoparticles had multiple self-assembled Au nanoparticles. Due to their outstanding electroconductivity and large surface area, they could significantly increase electron transfer and improve assay sensitivity of the proposed immunosensor [25–27]. While, the coated BSA layer of flower-like Au@BSA nanoparticles could serve as a multifunctional platform for easily conjugating a large number of luminol and anti-SARSR-CoV-2 antibodies, leading to a more sensitive detection of the target, thanks to its advantageous functional groups (–COOH, $–NH_2$, and –SH) [21,26]. Additionally, EDS analysis and FT-IR were also used to characterize the produced Au@BSA. The EDS examination revealed the presence of gold, carbon, nitrogen, and oxygen components (Fig. 1B), confirming that the Au@BSA nanoparticles were successfully constructed. As shown in Fig. 1C the typical stretching vibrations of –OH and –NH caused the wide peak at 3450 cm^{-1}, and the peak at 1520 cm^{-1} was also caused by –NH vibration. Furthermore, the characteristic peaks at 1646 and 1172 cm^{-1} were due to the –COO group vibration, implying that the synthesized Au@BSA could provide a variety of functional groups, including –COOH and $–NH_2$ groups.

3.2. Electrochemical characters of the immunosensor

Each step of functionalization and evaluation of the antibody-

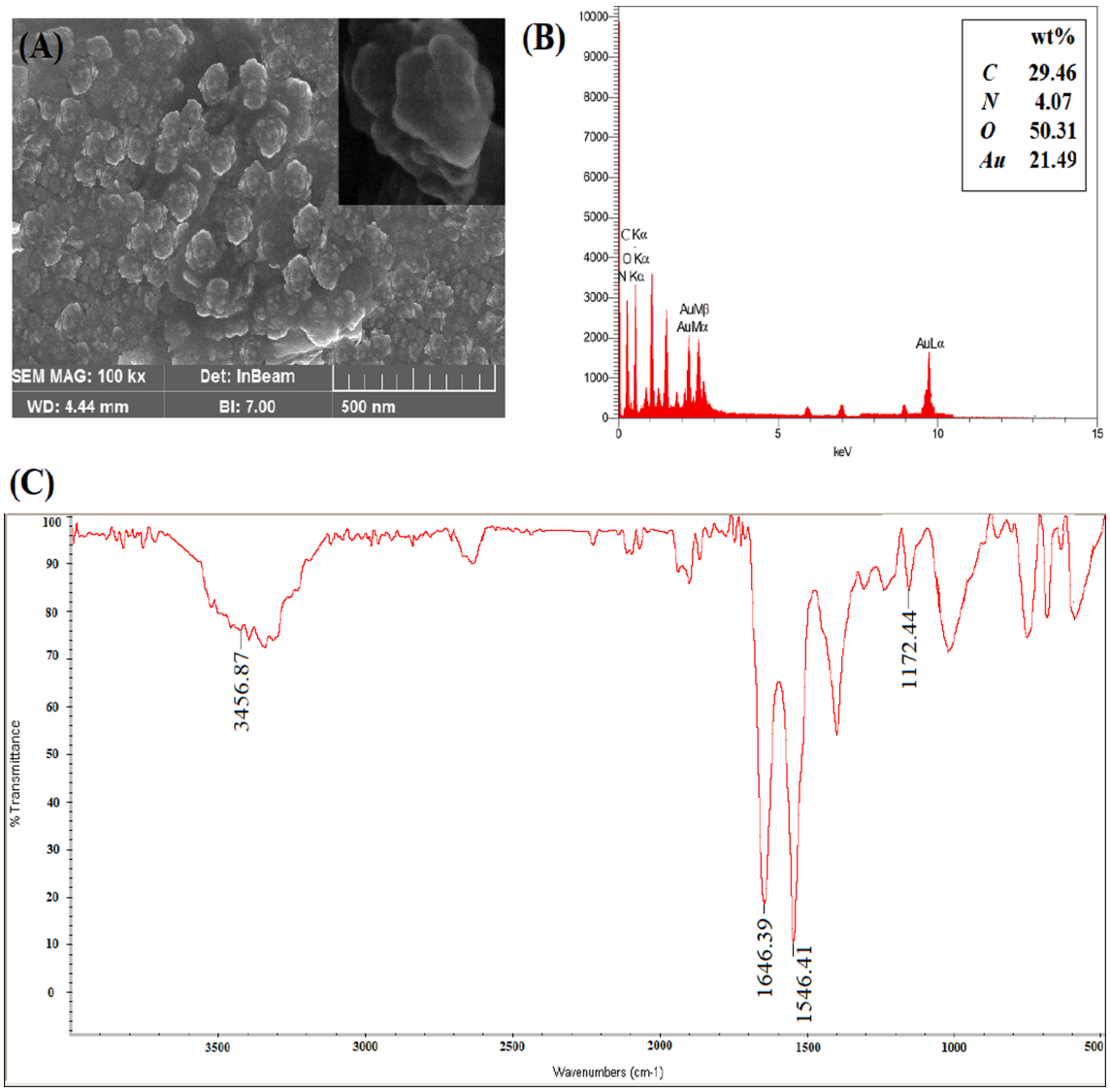

Fig. 1. (A) FESEM image of flower-like Au@BSA; (B) EDS analysis of Au@BSA nanoparticles; (C) FT-IR spectra of Au@BSA.

antigen interaction onto the surfaces of the sandwich immunosensor was characterized with cyclic voltammetry (CV) and electrochemical impedance spectroscopy (EIS) to further verify the fabrication process, as shown in Fig. 2. All CV and EIS measurements were performed in PBS solution (pH = 7.5), containing 0.1 M KCl and 5 mM $[Fe(CN)_6]^{3-/4-}$.

The ferri/ferrocyanide electron transfer kinetics alter from one step to the next, as seen by cyclic voltammograms (Fig. 2A). The ferri/ferrocyanide electron transfer kinetics of the bare GCE has a well-defined reversible peak. The peak current was enhanced when Au NPs were deposited on the electrode due to Au NPs' excellent electron transfer ability (curve b). After modification with MUA/MPA, the peak currents decreased confirming the modification of the electrode surface. modification with EDC/NHS and further on Ab_1 also led to a decrease in the current intensities confirming the successful immobilization of the capture antibody. The addition of SARS-CoV-2 also dropped the peak current of the CV curves. The addition of the produced nanocomposite also had a decreasing effect on the current intensity of the CV curves. All these results indicate that the proposed immunosensor has been successfully built.

Moreover, Fig. 2B clearly shows that the EIS of the bare GCE has a low electron transfer resistance. After depositing Au-Nps, a substantially smaller resistance (curve b) was detected, which was attributed to Au-Nps good electron transfer capacity and excellent conductivity. The diameter of the semicircle and electron transfer resistance increased after modification of the surface with MUA-MPA (curve c), antibody1 (curve d), and SARS-CoV-2 antigen curve e) due to the resistance of non-conductive bioactive compounds. When Luminol-Au@BSA-Ab_2 (curve f) was dropped on the electrode, the diameter of the semicircular in the EIS increased even more. This result confirms the CV data, indicating that the sandwich immunosensor was successfully assembled.

3.3. Optimization of analytical conditions

A series of optimization experiments were done based on sandwiched immunoassay to improve COVID-19 detection capability. The intensity of the ECL signal was studied against the incubation time of Ab_1 for 75 min in time intervals of 15 min. As can be seen from Figure S1a the intensity of the signals increased with the increasing time of incubation to 60 min and reduced afterwards suggesting that the optimum time for its incubation could be 60 min. Further more the ECL intensity was investigated against the reaction time between the analyte and Ab_1 where results suggested that a good-enough signal can be generated after 45 min (Figure S1b). The incubation time of the reporter nanocomposite was also investigated for a better signal intensity. As depicted in Figure S1c the optimum duration for this reaction was found to be 60 min.

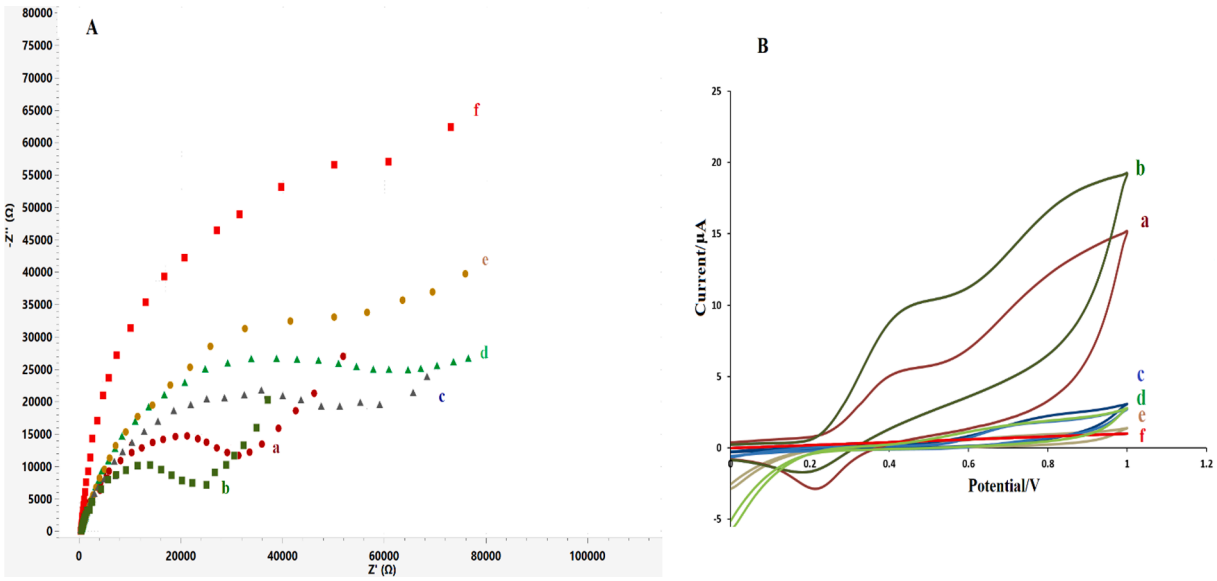

Fig. 2. (A) The Nyquist plots and; (B) Cyclic voltammograms of different modification steps in the 5 mM $K_3Fe(CN)_6$-$K_4Fe(CN)_6$ and 0.1 mol/L KCl system for various electrodes: (a) GCE, (b) GCE/AuNps, (c) GCE/AuNps/MUA-MPA, (d) GCE/AuNps/MUA-MPA/Ab1, (e) GCE/AuNps/MUA-MPA/Ab_1/BSA/SARS-CoV-2 antigen (f) GCE/AuNps/MUA-MPA/Ab_1/BSA /SARS-CoV-2 antigen/Luminol-Au @BSA-Ab_2.

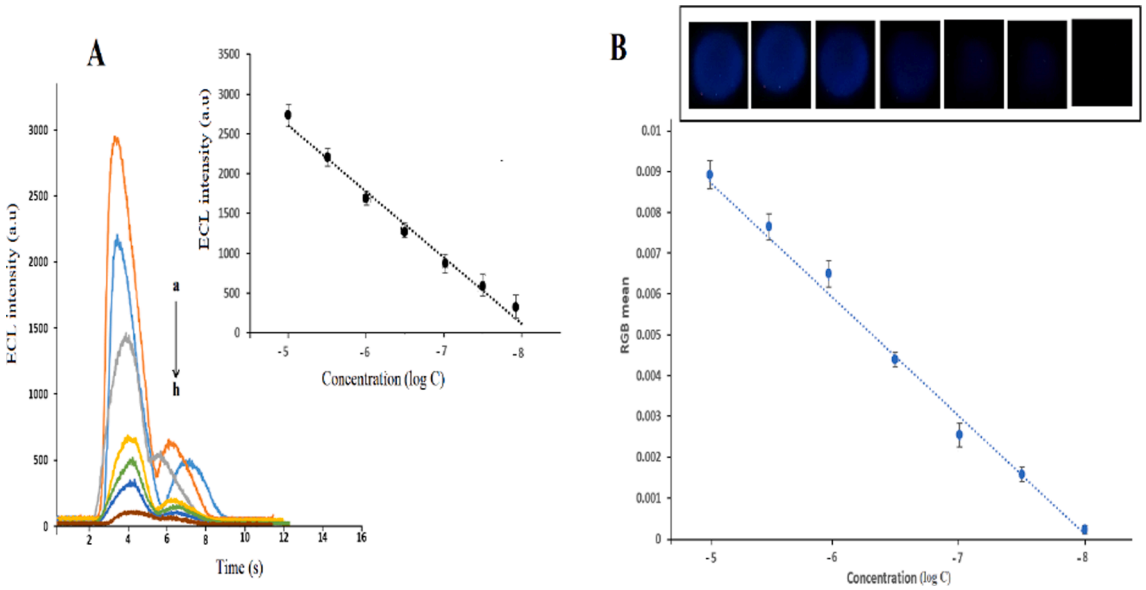

Fig. 3. (A) ECL response of the different concentrations of SARS-CoV-2 antigen (from curve a to curve h 10^{-5}, 2×10^{-6}, 10^{-6}, 2×10^{-7}, 1.5×10^{-7}, 10^{-7}, 10^{-8} g mL^{-1}, and without target). Inset shows the linear relationship between ECL intensity and the concentration of SARS-CoV-2 antigen. (B) RGB responses extracted from digital images in different concentrations (10^{-5}, 2×10^{-6}, 10^{-6}, 2×10^{-7}, 1.5×10^{-7}, 10^{-7}, 10^{-8} g mL^{-1}).

Figure S2a shows the relationship between ECL intensity and H_2O_2 concentration at ECL immunosensor. The ECL intensity were directly related to the H_2O_2 concentration at modified electrode, due to the more excited state of [Luminol]* produced with increasing H_2O_2 concentration. The ECL intensity increased and stabilized at 10^{-4} M of H_2O_2 and decreased with further concentration of H_2O_2.

The relationship between the ECL intensity and pH value was investigated over a pH range of 7.0 to 9.5. Figure S2b shows that the ECL signal increased considerably with the increase in pH from 7.0 to 8.5 and then decreased. The maximum ECL intensity was observed at pH 8.5. Thus, phosphate buffer solution of pH 8.5 was chosen for further ECL immunosensor determination.

3.4. Determination of SARS-CoV-2 antigen using the fabricated ECL immunosensor

The performance of the ECL immunosensor was further assessed by evaluating the ECL response at various concentrations of the SARS-CoV-2 antigen. Under the optimized conditions, the sandwich ECL biosensor was utilized to detect SARS-CoV-2 antigen. Fig. 3A depicted that the ECL signal intensity increased as the concentrations of SARS-CoV-2 antigen increased from 10 ng mL^{-1} to10 μg mL^{-1}. Furthermore, the change in ECL signal intensity was linearly related to antigen concentration, with a linear relationship of $y = -415.54x + 3015.9$, $R^2 = 0.9823$ ((inserted picture of Fig. 3A)). The LOD was calculated to be 1.93 ng mL^{-1} using the limit of detection (LOD) = 3 σ/k.

Moreover, visual detection of target was investigated for further

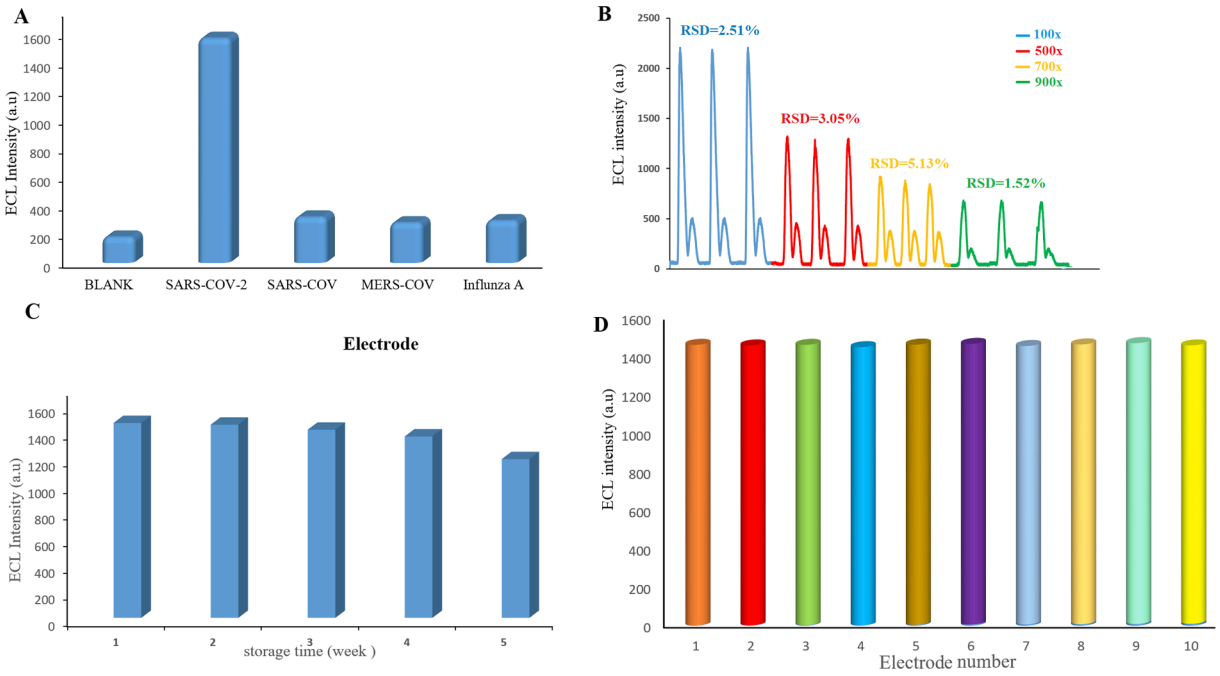

Fig. 4. (A) The selectivity of the ECL biosensor, (B) The ECL curves of the ECL biosensor for detecting SARS-CoV-2 antigen with various concentrations under three potential scans, (C) the long-term stability of the immunosensor, (D) reproducibility of the sensor using ten identical modified electrodes.

application of this system. The ECL images were collected by the smartphone camera and the image color was analyzed. The dataset was then transferred to a computer for further processing with MATLAB (R2016b, MathWorks Inc.). The region of interest (ROI) is the region where the color change occurs due to the reaction of the mixtures. To extract the ROI, several image processing methods need to be applied sequentially including grayscale conversion, thresholding, binarizing, masking, contour detection and noise removal. The extracted ROI was then masked with original images to extract the RGB features. Finally, RGB responses of the digital images in different concentration of target were extracted and illustrated in Fig. 3B.

3.5. *Specificity, stability, and reproducibility*

Stability, selectivity, reproducibility, and long-term stability of the biosensing device are important for use in clinical diagnosis. So, the ECL immunosensor's selectivity for the SARS-CoV-2 antigen should be examined. We compared the sensor's specificity to that of other related viruses, including SARS-CoV, MERS-CoV, and influenza A. The biosensor was immersed in 100 times SARS-CoV-2, 100 X SARS-CoV, 100 X MERS-CoV, 100 X influenza, and blank before being modified with Au@BSA-Luminol-Ab_2. The biosensor processed by SARS-CoV-2 antigen showed a significant difference compared to the biosensor processed by other viruses, as shown in Fig. 4A. As a result, the biosensor has excellent selectivity.

The ECL stability of the proposed sandwich immunosensor was examined at various SARS-CoV antigen concentrations (10^{-6}, 2×10^{-7}, 1.5×10^{-7}, 10^{-7} g mL^{-1}) under successive three potential scans (Fig. 4B). It was discovered that the ECL signal enhanced when the quantity of SARS-CoV-2 spike protein increased. Furthermore, ECL curves were relatively stable at all concentrations. The relative standard deviation (RSD) for SARS-CoV-2 spike protein detection was 2.51%, 3.05%, 5.13%, and 1.52%, respectively, indicating that the as-prepared ECL immunosensor has excellent stability. The ability of the created immunosensor for long-term cyclic use was also investigated since this factor was an important parameter for the immunosensors application. The ECL responses of the developed immunosensor could keep their ECL signal after four weeks (81.45%) when stored at 4 ^{0}C, as shown in Fig. 4C. Also, the biosensor's (GCE/AuNps/MUA-MPA/Ab_1/BSA) and produced electrodes for measuring SARS-CoV-2 antigen (1 μg mL^{-1}). The RSD was calculated to be 5.75%, indicating that the biosensor is repeatable (Fig. 4D).

Table 1
Clinical samples were analyzed using the proposed sandwich ECL immunosensor and RT-PCR.

Sample	This sensor	RT-PCR	CT value
Patient 1	Positive	Positive	19.1
Patient 2	Positive	Positive	18.8
Patient 3	Positive	Positive	22.3
Patient 4	Positive	Positive	15.7
Patient 5	Positive	Positive	18.4
Patient 6	Positive	Positive	21.9
Patient 7	Negative	Negative	No CT
Patient 8	Negative	Negative	No CT
Patient 9	Negative	Negative	No CT
Patient 10	Negative	Negative	No CT

3.6. *Clinical samples testing in pharyngeal swabs*

The direct identification of SARS-CoV-2 infected patients would be ideal for this sensing technology. So, saliva and nasopharyngeal swabs from ten positive and negative human subjects were examined with GCE/AuNps/MUA-MPA/Ab_1/BSA/target/Luminol-Au@BSA-Ab_2 our proposed immunosensor and the gold-standard RT-PCR, respectively, to assess the efficiency of the created sandwich Immunosensor using clinical samples. As shown in Table 1, our sensor can produce results that are comparable to gold-standard RT-PCR methods, but much faster. Fig. 5 shows the ECL response of the GCE/AuNps/MUA-MPA/Ab1/BSA immunosensor incubated in pharyngeal swabs of patients (without any treatment) and then modified with Luminol-Au@BSA-Ab_2. Photomultiplier tubes (PMT) and smartphones as detectors were used to measure ECL signals derived from sandwich immunosensor.

For further investigation, the signal response of various concentrations of SARS-CoV-2 antigen added in pharyngeal swabs according to the standard addition method was detected in recovery studies. The

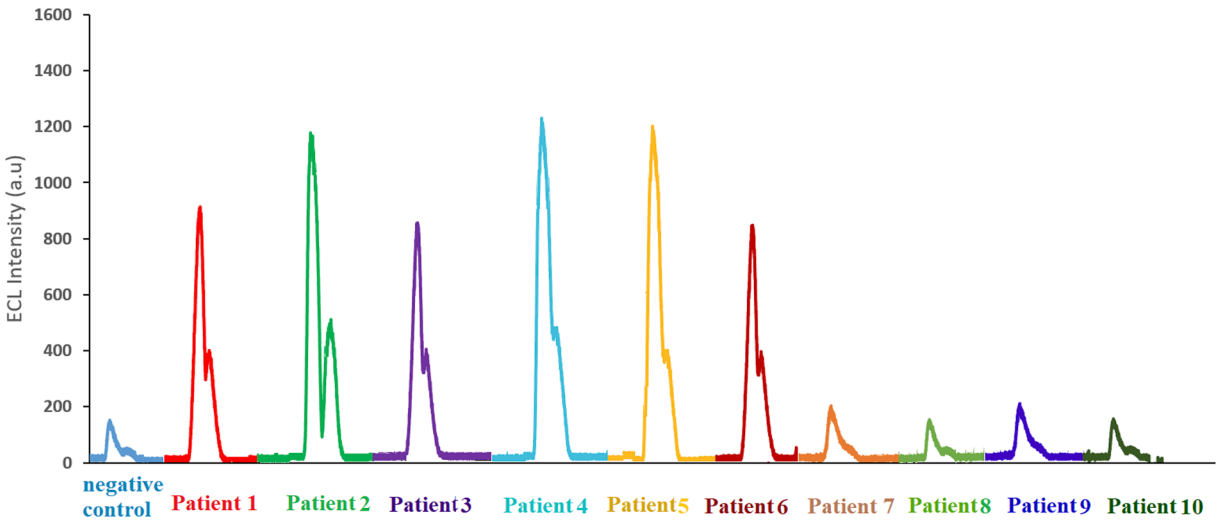

Fig. 5. The ECL signal of the ten clinical samples, using the proposed sandwich ECL immunosensor collected with PMT.

Table 2
Recovery results for the assay of proposed sandwich ECL immunosensor in pharyngeal swabs.

Sample	add	Found	Recovery%	RSD%(n = 3)
1	2 μg mL^{-1}	1.92 μg mL^{-1}	96	1.41
2	1 μg mL^{-1}	0.93 μg mL^{-1}	93	4.94
3	200 ng mL^{-1}	197.2 ng mL^{-1}	98.6	3.53
4	150 ng mL^{-1}	148.65 ng mL^{-1}	99.1	4.24

experimental recoveries ranged from 93% to 99.1%, with RSD values ranging from 1.41% to 4.94%, as shown in Table 2.

4. Conclusions

In this study, a sandwich ECL immunosensor for sensitive diagnosis of SARS-CoV-2 antigens was proposed based on flower-like Au@BSA nanoparticles. Because of their notable electroconductivity, good biocompatibility, and large surface area, flower-like Au@BSA nanoparticles not only have sufficient binding sites for loading plenty of Ab_2 but also adsorb large amounts of luminol molecules, resulting in enhancement of luminol ECL intensity, as well as good stability, excellent reproducibility, favorable selectivity, and a wide dynamic range of this developed immunosensor. The fast (90 min) and sensitive detection of SARS-CoV-2 antigens was recorded with a detection limit of 1.93 ng mL^{-1}. In addition, this sandwich ECL sensor is capable of detecting spike protein antigen of SARS-CoV-2 in real nasal swabs from patients and has an acceptable sensitivity and specificity. Significantly, the ECL images can be quickly recorded using a smartphone, and the results for SARS-CoV-2 detection were outstanding. The smartphone-based sensor platform is a field-deployable device that is portable, cost-effective, and user-friendly. In the future, it may be a useful tool for the early identification of SARS-CoV-2.

Declaration of Competing Interest

The authors declare that they have no known competing financial interests or personal relationships that could have appeared to influence the work reported in this paper.

Acknowledgements

The authors of this paper would like to express their gratitude to the Iran National Science Foundation and Chinese Academy of Sciences (INSF 99008701, CAS-VPST Silk Road Science, Found 2021, GJHZ202125) and for the financial support. We also gratefully acknowledge the support from the University of Tehran.

Appendix A. Supplementary material

Supplementary data to this article can be found online at https://doi.org/10.1016/j.bioelechem.2022.108161.

References

[1] M.M. Hassan, F.S. Sium, F. Islam, S.M. Choudhury, A review on plasmonic and metamaterial based biosensing platforms for virus detection, Sens. Bio-Sens. Res. 33 (2021), 100429, https://doi.org/10.1016/j.sbsr.2021.100429.
[2] E. Sánchez-Báscones, F. Parra, M.J. Lobo-Castañón, Aptamers against viruses: selection strategies and bioanalytical applications, TrAC Trends Anal. Chem. 143 (2021) 116349.
[3] Z. Zhao, C. Huang, Z. Huang, F. Lin, Q. He, D. Tao, N. Jaffrezic-Renault, Z. Guo, Advancements in electrochemical biosensing for respiratory virus detection: A review, TrAC Trends Anal. Chem. 139 (2021) 116253.
[4] M. Sher, A. Faheem, W. Asghar, S. Cinti, Nano-Engineered Screen-Printed Electrodes: A dynamic tool for detection of Viruses, TrAC Trends Anal. Chem. 143 (2021) 116374.
[5] E. Sobhanie, F. Faridbod, M. Hosseini, M. Ganjali, An Ultrasensitive ECL Sensor Based on Conducting Polymer/Electrochemically Reduced Graphene Oxide for Non-Enzymatic Detection in Biological Samples, ChemistrySelect 5 (17) (2020) 5330–5336.
[6] A. Karimi, S. Husain, M. Hosseini, P.A. Azar, M. Ganjali, A sensitive signal-on electrochemiluminescence sensor based on a nanocomposite of polypyrrole-Gd 2 O 3 for the determination of L-cysteine in biological fluids, Microchimica Acta 187 (7) (2020) 1–9.
[7] F. Salehnia, M. Hosseini, M.R. Ganjali, Enhanced electrochemiluminescence of luminol by an in situ silver nanoparticle-decorated graphene dot for glucose analysis, Anal. Methods 10 (5) (2018) 508–514.
[8] Z. Fan, B. Yao, Y. Ding, D. Xu, J. Zhao, K. Zhang, Rational engineering the DNA tetrahedrons of dual wavelength ratiometric electrochemiluminescence biosensor for high efficient detection of SARS-CoV-2 RdRp gene by using entropy-driven and bipedal DNA walker amplification strategy, Chem. Eng. J. 427 (2022), 131686.
[9] Z. Fan, B. Yao, Y. Ding, J. Zhao, M. Xie, K. Zhang, Entropy-driven amplified electrochemiluminescence biosensor for RdRp gene of SARS-CoV-2 detection with self-assembled DNA tetrahedron scaffolds, Biosens. Bioelectron. 178 (2021), 113015.
[10] B. Mojsoska, S. Larsen, D.A. Olsen, J.S. Madsen, I. Brandslund, F.A.a. Alatraktchi, Rapid SARS-CoV-2 Detection Using Electrochemical Immunosensor, Sensors, 2021. **21**(2), p. 390.
[11] L. Fabiani, M. Saroglia, G. Galatà, R. De Santis, S. Fillo, V. Luca, G. Faggioni, N. D'Amore, E. Regalbuto, P. Salvatori, G. Terova, D. Moscone, F. Lista, F. Arduini, Magnetic beads combined with carbon black-based screen-printed electrodes for COVID-19: A reliable and miniaturized electrochemical immunosensor for SARS-CoV-2 detection in saliva, Biosens. Bioelectron. 171 (2021), 112686, https://doi.org/10.1016/j.bios.2020.112686.
[12] W. Zhu, X. Lv, Q. Wang, H. Ma, D. Wu, T. Yan, L. Hu, B. Du, Q. Wei, Ru (bpy) 3 2+/ nanoporous silver-based electrochemiluminescence immunosensor for alpha fetoprotein enhanced by gold nanoparticles decorated black carbon intercalated reduced graphene oxide, Sci. Rep. 6 (1) (2016) 1–9.

[13] E.B. Aydın, M. Aydın, M.K. Sezgintürk, New Impedimetric sandwich immunosensor for ultrasensitive and highly specific detection of spike receptor binding domain protein of SARS-CoV-2, ACS Biomater. Sci. Eng. 7 (8) (2021) 3874–3885, https://doi.org/10.1021/acsbiomaterials.1c00580.

[14] E.B. Aydın, M. Aydın, M.K. Sezgintürk, Highly selective and sensitive sandwich immunosensor platform modified with MUA-capped GNPs for detection of spike Receptor Binding Domain protein: A precious marker of COVID 19 infection, Sens. Actuators, B 345 (2021), 130355, https://doi.org/10.1016/j.snb.2021.130355.

[15] H. Zhao, F. Liu, W. Xie, T.-C. Zhou, J. OuYang, L. Jin, H. Li, C.-Y. Zhao, L. Zhang, J. Wei, Y.-P. Zhang, C.-P. Li, Ultrasensitive supersandwich-type electrochemical sensor for SARS-CoV-2 from the infected COVID-19 patients using a smartphone, Sens. Actuators, B 327 (2021), 128899, https://doi.org/10.1016/j.snb.2020.128899.

[16] W. Gao, K. Muzyka, X. Ma, B. Lou, G. Xu, A single-electrode electrochemical system for multiplex electrochemiluminescence analysis based on a resistance induced potential difference, Chem. Sci. 9 (16) (2018) 3911–3916.

[17] M. Hosseini, M.R. Karimi Pur, P. Norouzi, M.R. Moghaddam, F. Faridbod, M. R. Ganjali, J. Shamsi, Enhanced solid-state electrochemiluminescence of Ru (bpy) $_3^{2+}$ with nano-CeO_2 modified carbon paste electrode and its application in tramadol determination, Anal. Methods (2015).

[18] Ö.B. Mercan, V. Kılıç, M. Şen, Machine learning-based colorimetric determination of glucose in artificial saliva with different reagents using a smartphone coupled μPAD, Sens. Actuators, B 329 (2021), 129037.

[19] V. Kılıç, N. Horzum, M.E. Solmaz, From sophisticated analysis to colorimetric determination: Smartphone spectrometers and colorimetry, Color Detection (2018) 1–19.

[20] W. Li, R. Zhang, H. Wang, W. Jiang, L. Wang, H. Li, T. Wu, Y. Du, Digital image colorimetry coupled with a multichannel membrane filtration-enrichment technique to detect low concentration dyes, Anal. Methods 8 (14) (2016) 2887–2894.

[21] A. Zhang, H. Xiang, X. Zhang, W. Guo, E. Yuan, C. Huang, N. Jia, A novel sandwich electrochemiluminescence immunosensor for ultrasensitive detection of carbohydrate antigen 19–9 based on immobilizing luminol on Ag@ BSA core/shell microspheres, Biosens. Bioelectron. 75 (2016) 206–212.

[22] A. Zhang, W. Guo, H. Ke, X. Zhang, H. Zhang, C. Huang, D. Yang, N. Jia, D. Cui, Sandwich-format ECL immunosensor based on Au star@ BSA-Luminol nanocomposites for determination of human chorionic gonadotropin, Biosens. Bioelectron. 101 (2018) 219–226.

[23] M. Naderi, M. Hosseini, M.R. Ganjali, Naked-eye detection of potassium ions in a novel gold nanoparticle aggregation-based aptasensor, Spectrochim. Acta Part A: Mol. Biomol. Spectrosc. 195 (2018) 75–83, https://doi.org/10.1016/j.saa.2018.01.051.

[24] N. Fakhri, M. Hosseini, O. Tavakoli, Aptamer-based colorimetric determination of Pb2+ using a paper-based microfluidic platform, Anal. Methods 10 (36) (2018) 4438–4444, https://doi.org/10.1039/C8AY01331D.

[25] X. Ning, H. Bao, X. Liu, H. Fu, W. Wang, J. Huang, Z. Zhang, Long-term in vivo CT tracking of mesenchymal stem cells labeled with Au@ BSA@ PLL nanotracers, Nanoscale 11 (43) (2019) 20932–20941.

[26] A. Zhang, C. Huang, H. Shi, W. Guo, X. Zhang, H. Xiang, T. Jia, F. Miao, N. Jia, Electrochemiluminescence immunosensor for sensitive determination of tumor biomarker CEA based on multifunctionalized Flower-like Au@ BSA nanoparticles, Sens. Actuators, B 238 (2017) 24–31.

[27] Z. Wang, H. Wu, H. Shi, M. Wang, C. Huang, N. Jia, A novel multifunctional biomimetic Au@ BSA nanocarrier as a potential siRNA theranostic nanoplatform, J. Mater. Chem. B 4 (14) (2016) 2519–2526.